Article

Far-Field Wireless Power Transfer for the Internet of Things

Tasin Nusrat [1], Sayan Roy [1], Abbas Ali Lotfi-Neyestanak [2] and Sima Noghanian [3],*

1. Department of Electrical Engineering and Computer Science, South Dakota Mines, Rapid City, SD 57701, USA
2. Medical Cytometrix Inc., Surrey, BC V3X 2Y1, Canada
3. CommScope Ruckus Networks, Sunnyvale, CA 94089, USA
* Correspondence: sima_noghanian@ieee.org

Abstract: A complete end-to-end far-field wireless power transfer (WPT) is proposed and studied in this paper for the application of the Internet of Things (IoT) at the industrial, scientific, and medical (ISM) band of 2.4 GHz. The radiative WPT has achieved a remarkable attraction for the capability to transfer power in the long range. We propose two approaches. In the first approach, a 2×4 microstrip patch transmitter antenna array with a high gain and a narrow beamwidth is proposed that is rotated toward the IoT device using a small stepper motor. The performance of the rectifier in the receiving circuit was separately analyzed, and 17.54% efficiency was achieved with a load of $0.6 \text{ k}\Omega$ for the circuit, while the input power was 10 dBm. The overall system test was performed and the targeted result was investigated considering the distance between the transmitter and the receiver, and an input radio frequency (RF) power of 5 dBm to 15 dBm at 2.4 GHz. The second approach uses a 1×4 transmitter antenna array fed through a Butler matrix to provide four individual beams with a $22.5°$ angular separation, and $90°$ total angular coverage. The goal was to focus the power into four angular locations and to reduce the power waste in other directions. A mobile app was developed to control the direction of the beam. A system efficiency of as much as 19% was measured for an input RF power of 0 dBm and a resistive load of $62 \text{ k}\Omega$.

Keywords: wireless power transfer (WPT); far-field RF energy transfer; array antenna; efficient rectenna; IoT

1. Introduction

Wireless power transfer (WPT) has gained incredible attention due to the development of numerous Internet of things (IoT) devices [1] and batteryless autonomous wireless sensor nodes. The Transform Insights TAM Forecast Database predicts that the number of IoT devices will increase to 24.1 billion by 2030 [2]. In recent years, the technology of WPT has also shown potential application in the field of biomedical implants, high-powered electric vehicles, portable smart devices, and radio-frequency identification (RFID). To satisfy the immense change in the wireless industry and IoT, efficient WPT has become one of the main challenges.

Over a number of decades, many methodologies have been applied based on implementing non-radiative and radiative techniques for executing the WPT technology. Although the non-radiative or near-field WPT based on capacitive, inductive, and strong resonant coupling has shown excellent commercial progress (e.g., charging mobile devices) [3], it is not always convenient because the power transfer efficiency drops quickly after a certain range. On the contrary, in the radiative or far-field WPT system, the energy is transferred through electromagnetic waves. This methodology can transfer enough power for long distances [4], but, it is not an easy task to transfer power in the far-field, as most of the energy is dissipated into the air. In addition, strict restrictions have been declared by the Federal Communications Committee (FCC) on the safety and exposures of RF signals [5].

Nikola Tesla was the first person to successfully transfer microwave signals over a long distance of about 48 km in 1896 [6]. In 1899, another keystone was achieved by

transmitting 100 MW of electric power to light 200 lamps over a distance of 40 m [6]. This technology required ample space, and it had potentially damaging effects on the environment. The milestone of converting microwaves to electricity was achieved by William Brown in 1964, where he used a rectenna to perform the conversion [7]. Since then, there has been a lot of research on improvements in five significant areas: novel transmitting and receiving antennas, power combining from multiple sources, impedance matching, different rectifying circuits, and circuit miniaturization [8]. One goal is to maximize power transfer efficiency.

When it comes to charging low-power sensors or IoT devices, it is important to focus the beam and to increase the transmitter gain, since the low-power sensors usually have a small and low-gain receiver antenna. Various methods are proposed in the literature. In [9] a Van Atta array of four slots, each fed by eight coaxial ports, working at the 5.8 GHz band is proposed. The array can collect and re-radiate the power impinging on it. An amplifier is added on the path to send more power back than the power received. This method provides up to a 118° scan; however, it requires the sensor to send power to the transmitter, so that the transmitter finds the direction and sends power to the sensor. Frequency scanning can be used when the receiver antennas have enough bandwidth. This method is proposed in [10]. The transmitter antenna is a half-width substrate integrated waveguide leaky-wave antenna that can cover an angular spread of 20° at 2.4 GHz and 74° at 2.5 GHz. The feeding is simple and the antenna is low profile, but the limitation is that the receiver needs to be able to receive power at a wider frequency band. A Rotman lens attached to eight Vivaldi antennas, working at a 33 GHz band, is proposed in [11]. The array is capable of directing the beam from −30° to +30°.

A phased array can provide a larger angular coverage; however, it will require a complex beam-forming network consisting of a power divider and multiple phase shifters. In [12], a phased array of circular polarized patch antennas is proposed that uses a pre-recorded look-up table to quickly search and find the proper phase for the desired beam direction. The array is designed for 5.2 GHz.

Another way of rotating a beam without a complex feed network is to use parasitic elements. In [13], an array of 3×3 of patch antenna elements is proposed. The center element is an active one, and the surrounding patches are acting as parasitic elements. Varactor diodes are needed to activate the parasitic elements. The simulation shows a scan capability from 60° to 90°.

In this work, a complete radiative wireless power transfer has been proposed. We propose two approaches. Both approaches use patch array antennas with a narrow beam. To cover the most angular area, in the first approach, a stepper motor is used to rotate the microstrip patch array, and it provides the beam rotation. The direction of the beam can be controlled via a mobile app. The second approach is for scenarios such as a cluster of closely located sensors. Four simultaneous beams can be generated through a Butler matrix. The aim is to transmit power in the far-field region in a realistic application, such as the IoT devices, via a narrow beam high-gain transmitter. The transmitting and receiving antennas and the rectifier module for each approach were designed, simulated, and fabricated. Table 1 provides a summary of the methods proposed in the related literature and the current work. In the remainder of this paper, we provide the following: The detailed hardware configuration is explained in Section 2, and the measured results and analysis are presented in Section 3. Finally, in Section 4 conclusions and a summary of the results are given.

Table 1. Wireless power transfer via directive beam methodology.

References	Transmitter Type, Frequency (GHz)	Angular Scan or Coverage (Degrees)
[9]	Van Atta and 4 slot array, 5.8	118
[10]	Leakywave, 2.4–2.5	74
[11]	Rotman lens and 1×8 Vivaldi array, 33	60
[12]	Timed shared beamforming 8×8 patch phased array, 5.745	Four beams at 45°, 135°, 225° and 315°
[14]	Circular polarized 4×8 patch array, 5.2	Look up table of phase
[13]	Electronically steered parasitic array 3×3 array, 2.45	30
This work, Approach I	Stepper motor and 2×4 patch array, 2.4	360
This work, Approach II	Butler matrix and 1×4 patch array, 2.4	90

2. Methodology and Design

To achieve higher efficiency, our approach is to use a directive transmitter and rotate the beam toward the IoT devices. To avoid a complex phased array feed network, minimize the cost, and control the direction of the beam, we considered two scenarios.

In the first scenario, we assume that the location of the receiving devices is known but does not have to be fixed. The first approach utilizes an array of antennas with a narrow beam that can be rotated toward the desired angle using a stepper motor. This system consists of an RF power source, a 2×4 transmitter array antenna, and a single receiver patch antenna integrated with a rectifier circuit (rectenna). An XBee module is connected to the stepper motor to control the motor wirelessly. XBee uses the XCTU software. A mobile app is developed to provide access to the stepper motor and to rotate the beam to the desired angle.

In the second scenario, we assume that the IoT devices are clustered in specific fixed locations with a small angular spread. To create multiple beams toward a few predefined angles, a Butler matrix is used. A Butler matrix is chosen since it does not need a complex beamforming network and high-loss phase shifters. However, it only provides a small number of predefined beam directions. It can send simultaneous power to multiple angles where the IoT devices may be located. In this approach, a 1×4 patch array was connected to the Butler matrix. At the receiver side, a single patch antenna and a rectifier was used to provide the DC power. A mobile application was developed for the easy control of the beams and the power level that is transferred.

It is possible to combine the two approaches. In this case, the array that is attached to the Butler matrix should be mounted on a stepper motor.

2.1. Approach I

2.1.1. The Transmitter System

The RF Power Source

The RF power source was a Keysight (Agilent) E4421B 250 kHz–3.0 GHz signal generator. The output power of the generator was measured for different magnitudes and frequency levels to confirm that they exactly matched the figures on the display of the generator. Additionally, a fixed-length coaxial cable of length 1 m was attached to the generator for delivering the RF signal to the transmitter. The cable loss at the ISM bands was measured to be 3 dB, and the output was adjusted accordingly during all the measurements.

The Microstrip Patch Array Antenna

We used a high-gain antenna array for the power transfer. This approach ensures the selected location receives maximum power and that no power is wasted in the various directions. The transmitter system comprised a 2×4 microstrip patch array antenna (MPAA), a stepper motor, a motor driver, and an Arduino controller, as shown in Figure 1a,b.

To transfer the power, the transmitter array has to be rotated in a proper azimuth direction where the sensor becomes aligned with the broadside of the array. Let's consider a case (I) when the array is mounted on a stepper motor in Figure 2a where an IoT device is placed at an angle to the left of the array; the array is rotated to directly face to IoT A. If IoT B is located at a different angle, we used a stepper motor to rotate the beam toward it. In Figure 2b, the array is properly aligned with the IoT B when the stepper motor is rotated precisely, using the knowledge of the angular position of the IoT sensors and the mobile app we developed. The user can define the period and the duration of powering up each sensor. The motor then will rotate periodically to send power to each IoT device. It should be noted here that the knowledge of the angular positions of the sensors is required to program the stepper motor's rotation. The use of a stepper motor gives us the ability to periodically rotate the beam and to provide power to sensors that are located at any angle with respect to the transmitter. The power provided to the sensors is not continuous, since the transmitter is rotated periodically.

In our laboratory test, the movement of the array was realized using a NEMA 23 stepper motor (1.9 N.m). The motor was controlled using a Toshiba stepper motor driver TB6600 and programmed using an Arduino microcontroller.

(a)   (b)
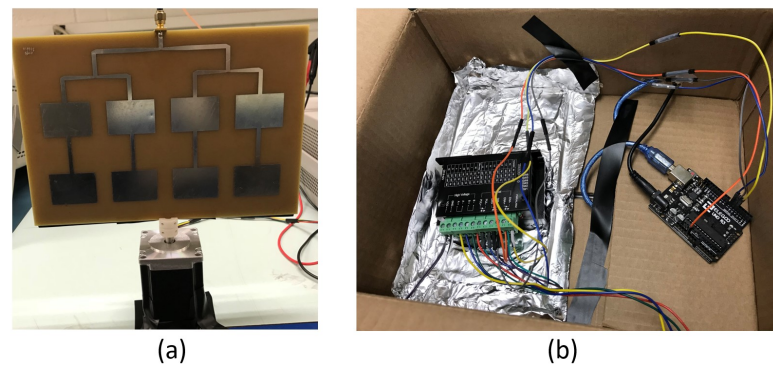
Figure 1. (**a**) Prototype of 2×4 MPAA, (**b**) stepper motor driver and controller circuit connected to the MPAA.

(a)   (b)
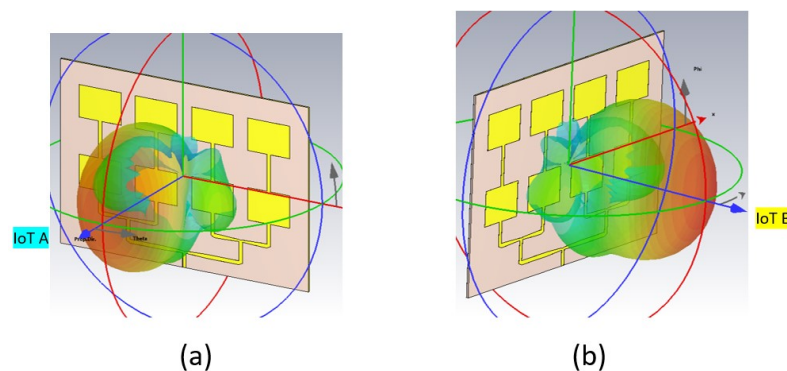
Figure 2. (**a**) Case I, (**b**) Case II.

2.1.2. The Receiver System
Receiving Antenna Design

The goal was to capture RF energy using a rectifier antenna, which is then converted to usable DC power. Considering the path loss, a compact size and a high-gain-receiving

antenna was needed [15,16]. A microstrip patch antenna (MPA) was proposed, which provides a small size, good radiation pattern, and high gain. The fabricated antenna is shown in Figure 3a. The patch antenna was fabricated using an LPKF S103 milling machine, and the antenna substrate was a double-sided Cu-cladded 1.57 mm thick FR4. The dimension of the patch antenna is extracted using the equations in [17], and all of the parameters are shown in Figure 3b.

Rectenna Design

The rectifier circuit is preferred to be in coplanar form, whereas the patch antenna is a microstrip. This is necessary to achieve a better form factor and to eliminate unwanted losses due to the transmission of signals through excess conductive areas without losing its performance and efficiency. This means that a co-planar waveguide (CPW) to microstrip transition is required to integrate the rectifier circuit with the patch antenna. Therefore, a CPW to microstrip transition was designed, and the antenna with the transition is shown in Figure 3c.

The saturation current is a critical parameter that impacts on the efficiency of diodes. Therefore, it is desirable to have diodes with a high saturation current, low junction capacitance, and low equivalent series resistance. Moreover, diodes with higher saturation current also yield a higher forward current, which is beneficial for load driving. However, a higher saturation current is usually found in larger diodes, which have higher junction and substrate capacitance. The latter two parameters can introduce increased power loss, where the benefit of a higher saturation current is lost. To address this, a Schottky detector diode from the HSMS-285x Series was used and integrated with a capacitor and a resistor.
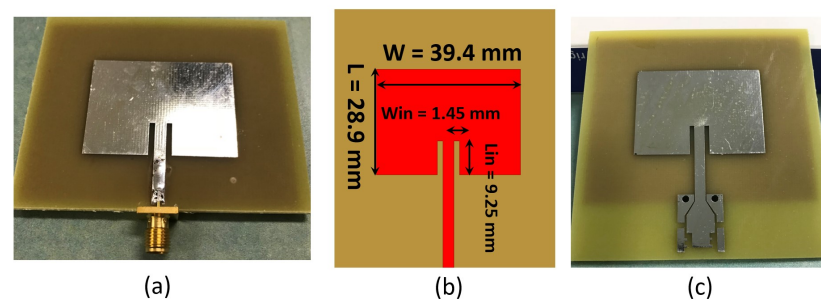
Figure 3. (**a**) Prototype of patch antenna, (**b**) Dimension of the printed MPA, (**c**) MPA with CPW transition.

2.2. Approach II

2.2.1. The Transmitter System

The transmitter consists of an RF power source, a 4×4 Butler matrix for beam-switching, a 1×4 microstrip antennas array, a microwave SP4T switch for beam-selection, a microcontroller to send selection commands to the switch, and a Bluetooth module to receive commands from a smartphone and to send commands to the microcontroller. The block diagram of the system is shown in Figure 4. All of the components other than the Butler matrix and antennas are off-the-shelf. We used an Arduino NANO as a single-board microcontroller. Because the microwave switch operates with 3.3 V, we used Massduino Arduino, which works with 3.3V logic instead of regular NANO. This microcontroller is similar to the Nano microcontroller and is capable of working in both 3.3 and 5 V logic. We also used nRF24L01, which is a single-chip radio transceiver for the 2.4–2.5 GHz ISM band. The transceiver consists of an integrated frequency synthesizer, a power amplifier, a crystal oscillator, a demodulator, and a modulator. Its output power, frequency channels, and protocol setup are programmable through an SPI interface, and it has a power amplifier and a low noise amplifier circuit on board. The RF power module has a maximum output power of 100 mW and was designed to operate in continuous wave (CW) mode. We used a simple XBee (HC-06) Bluetooth module to control and send commands to the system (turning on and off the module and controlling the switching time), using a smartphone.

For the SP4T switch, we used PE42441 (with the Evaluation board EK42441). The switch has an insertion loss of 0.8 dB and an isolation of 45 dB. The system works with a mobile application that has been designed for Android phones. The receiver consists of a microstrip antenna, a matching circuit, and a Schottky diode detector with an output filter.
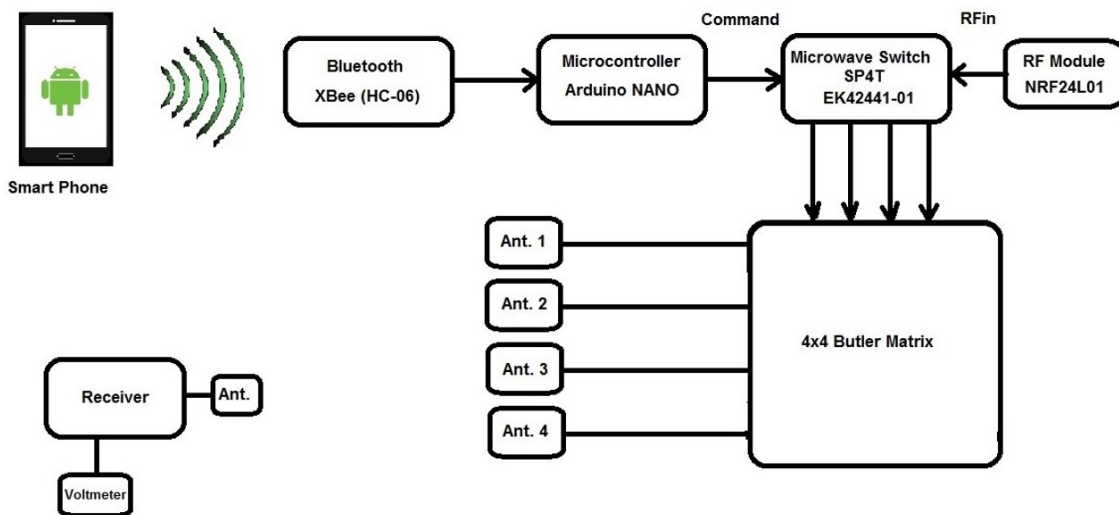

Figure 4. Block diagram for the intelligent wireless power transfer.

Antenna Design

A butterfly-shaped patch antenna (BSPA) design is proposed here by adding two circles at the bottom and one ellipse at the top of the usual patch antenna. The shape of the patch was modified to improve the gain and bandwidth. This new design shown in Figure 5 of the antenna was fabricated using an FR4 substrate with a 1.6 mm substrate thickness. The antenna design was used to create the array, as well as a single-element receiver antenna.

(a)   (b)
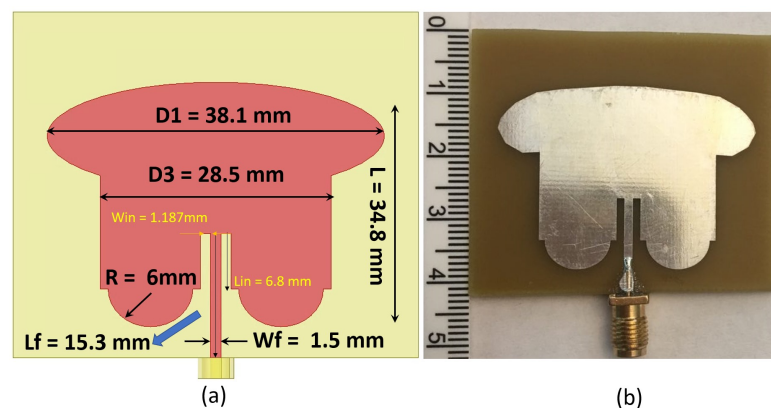
Figure 5. (**a**) Butterfly-shaped patch antenna, (**b**) Photograph of the fabricated antenna.

The Butler Matrix

The Butler matrix was first introduced by Jesse Butler and Ralph Lowe [18]. As seen in Figure 6a, the Butler matrix divides the input power into four outputs with the same amplitude but with a linear phase taper. Figure 6b shows how we can select different output beams by switching between different inputs (for each case, the other inputs are matched). A 4 × 4 Butler matrix is composed of four 3 dB/90° directional couplers and two 45° phase shifters. Two additional crossovers are needed when the matrix is integrated on the same plane as the radiating elements, forming a fully integrated multibeam linear array antenna. The outputs are linear combinations of the inputs and can be expressed as [19,20]:

$$1L = 1/4(A_1\angle 225° + A_2\angle 270° + A_3\angle 315° + A_4\angle 0°) \tag{1}$$

$$2R = 1/4(A_1\angle 270° + A_2\angle 45° + A_3\angle 180° + A_4\angle 315°) \tag{2}$$

$$2L = 1/4(A_1\angle 315° + A_2\angle 180° + A_3\angle 45° + A_4\angle 270°) \tag{3}$$

$$1R = 1/4(A_1\angle 0° + A_2\angle 315° + A_3\angle 270° + A_4\angle 225°) \tag{4}$$
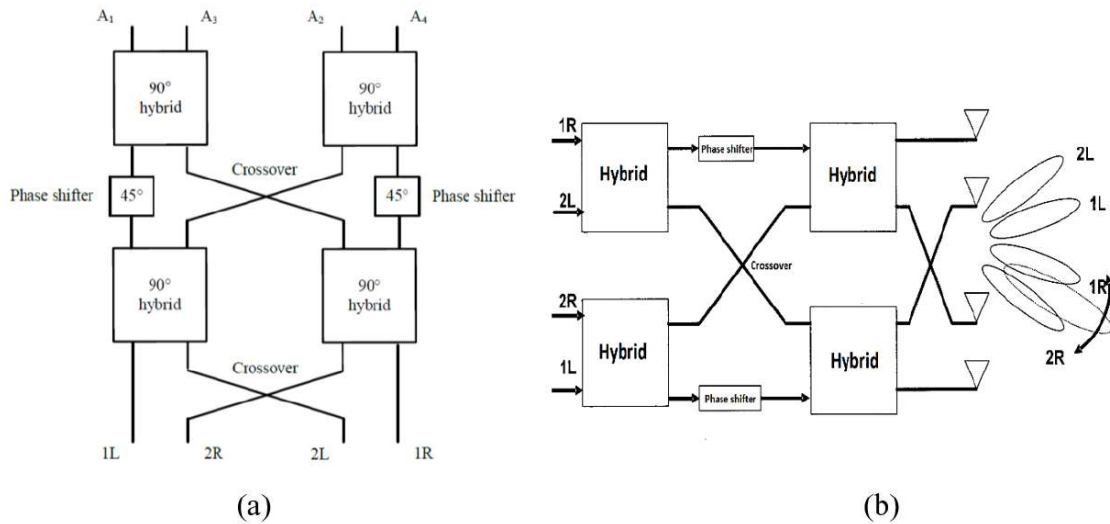
Figure 6. (**a**) A 4 × 4 Butler matrix block diagram, (**b**) Beam selection.

Each part of the building blocks of the Butler matrix is designed on an FR4 substrate with a dielectric constant of 4.4 and a substrate thickness of 1.6 mm. As already mentioned, a Butler matrix is composed of balanced hybrid couplers, 0 dB couplers (cross-overs), and phase shifters. A commercial finite element method simulation tool (ANSYS HFSS) was used to optimize the electromagnetic performances of the different building blocks. Figure 7 shows a schematic diagram of the fabricated Butler matrix. The overall system is shown in Figure 8.
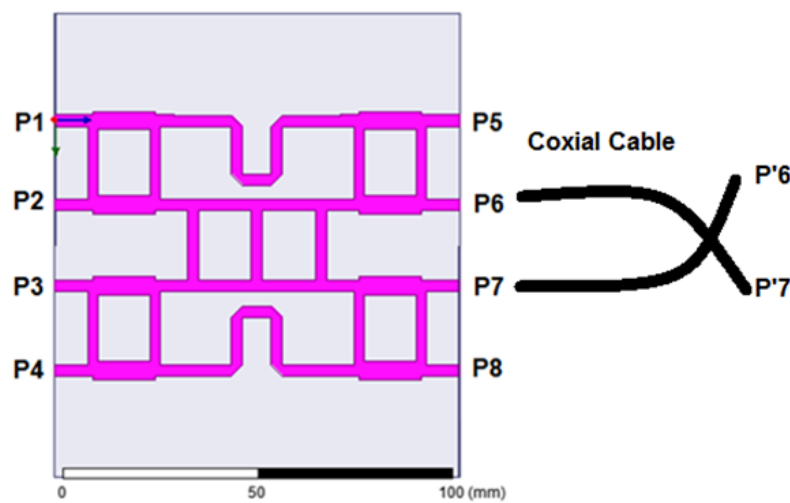
Figure 7. Schematic diagram of the Butler matrix.
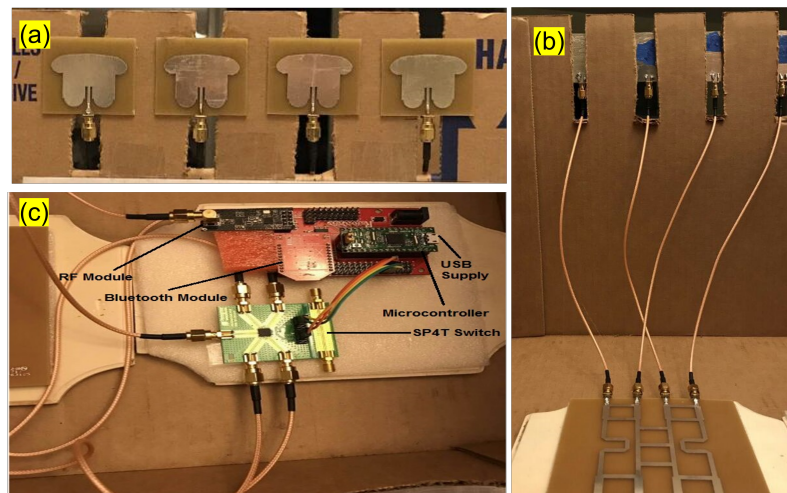
Figure 8. A complete system for approach II, (**a**) Front view consisting of 1×4 antenna array, (**b**) Back view showing array connected to the Butler matrix, (**c**) Control parts.

3. Result and Analysis

3.1. Approach I

3.1.1. Antennas

The reflection coefficient ($|S_{11}|$) of 2×4 MPAA was measured using a Keysight E5071C ENA Network Analyzer (300 kHz to 20 GHz). The simulated and measured values of ($|S_{11}|$) in decibels (dB) are shown in Figure 9. A very good matching can be observed at a bandwidth of between 2.4 GHz and 2.5 GHz. It should also be noted that the array was designed for maximum radiation along the broadside direction, i.e., the maximum direction of the radiation of the array is toward the normal direction to its surface. The simulated value of the realized gain is 9.63 dBi, with a side lobe level of better than 17.2 dB. The antenna was measured using a Satimo antenna measurement chamber. The measured gain was 9.3 dBi. The normalized measured radiation patterns are shown in Figure 10. The measured half-power beamwidth on the XZ plane ($\phi = 0°$) is 60° and the side lobe level is 19.6 dB. On the YZ plane ($\phi = 90°$), the half power beamwidth was measured at 33°, and the side lobe level was 14.5 dB.
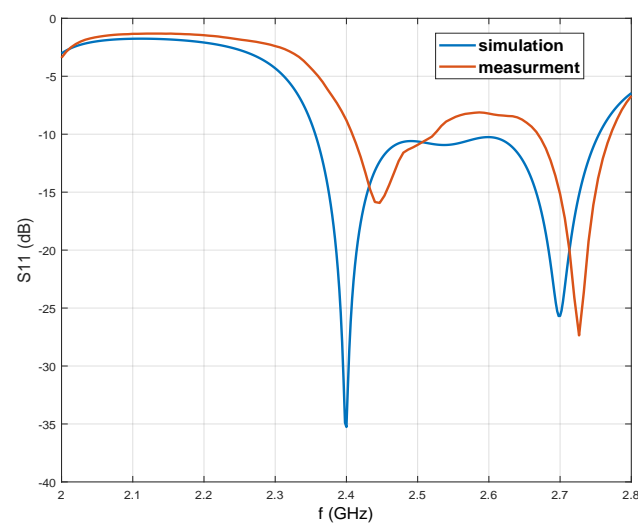
Figure 9. Simulated and measured reflection coefficient ($|S_{11}|$) of the 2×4 MPAA.

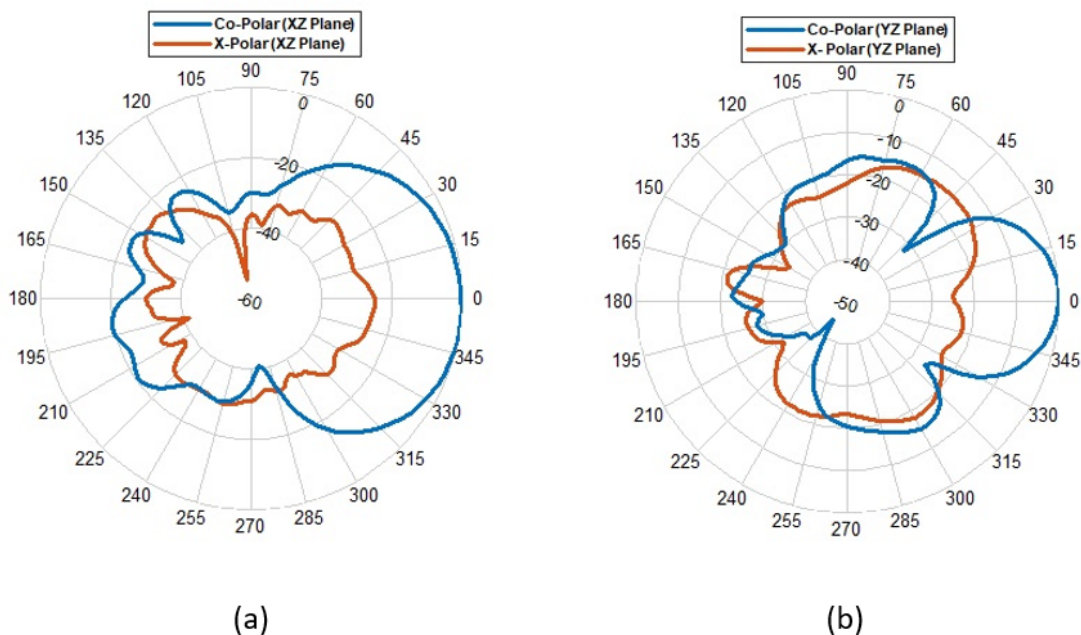**Figure 10.** Measured MPAA patterns (**a**) $\phi = 0°$, (**b**) $\phi = 90°$.

A single microstrip antenna (MPA) was used as the receiver. The simulated and measured patterns are depicted in Figure 11. The simulated realized gain was 2.9 dBi, and the measured gain was 2.7 dBi. The simulated and measured reflection coefficients ($|S_{11}|$) are shown in Figure 12, which demonstrates a good performance at the resonant frequency of 2.4 GHz.
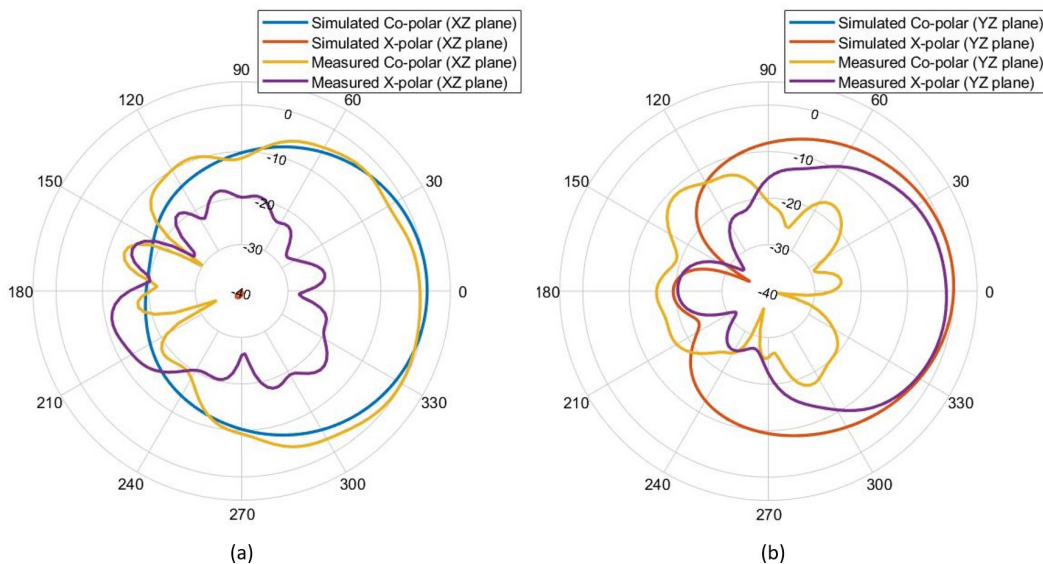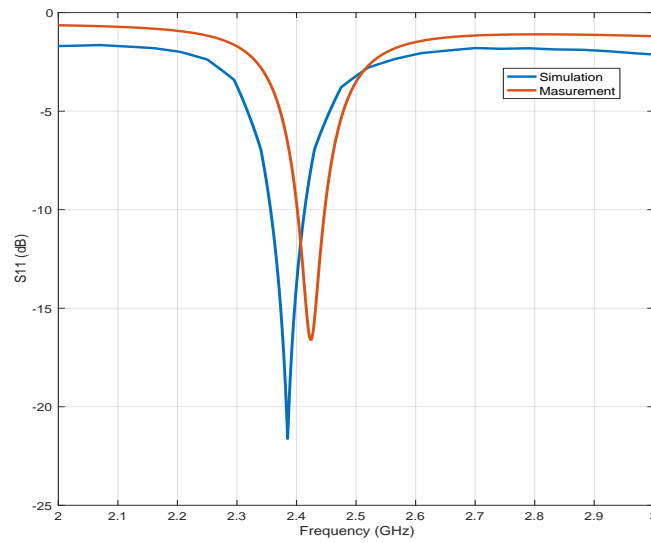

Figure 11. Simulated and measured MPA radiation patterns at 2.4 GHz (**a**) $\phi = 0°$, (**b**) $\phi = 90°$.

Figure 12. Simulated and measured reflection coefficient ($|S_{11}|$) of the inset-fed MPA.

3.1.2. The Rectifier Circuit

To evaluate the performance of the rectifier circuit, the DC voltage for different input power (P_m) levels for a range of resistive loads at the receiving end was measured, and the results are plotted in Figure 13. The calculated rectifier efficiency for different receiver resistive loads is shown in Figure 14. The best efficiency is 17.54%, while the resistive load was 0.6 kΩ and the input power was 10 dBm at 2.4 GHz. The remaining tests were conducted with this fixed resistive load of 0.6 kΩ, which mimics the IoT device.
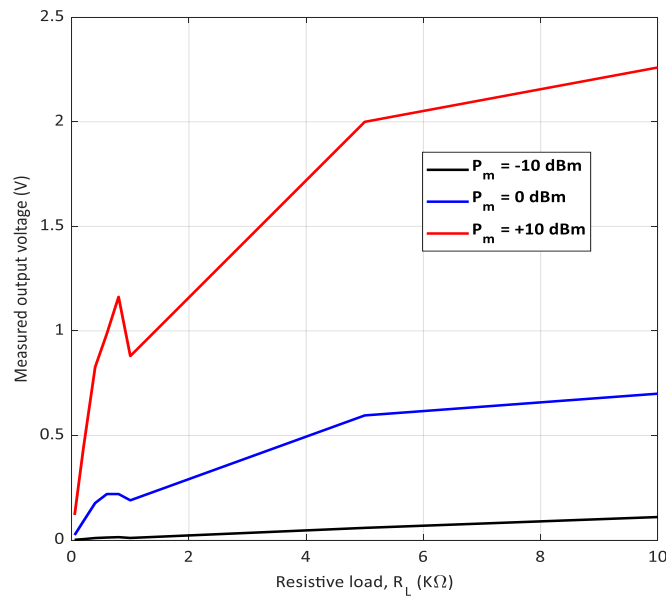
Figure 13. Output voltages at the load for different R_L and P_m for the rectifier circuit in Approach I.
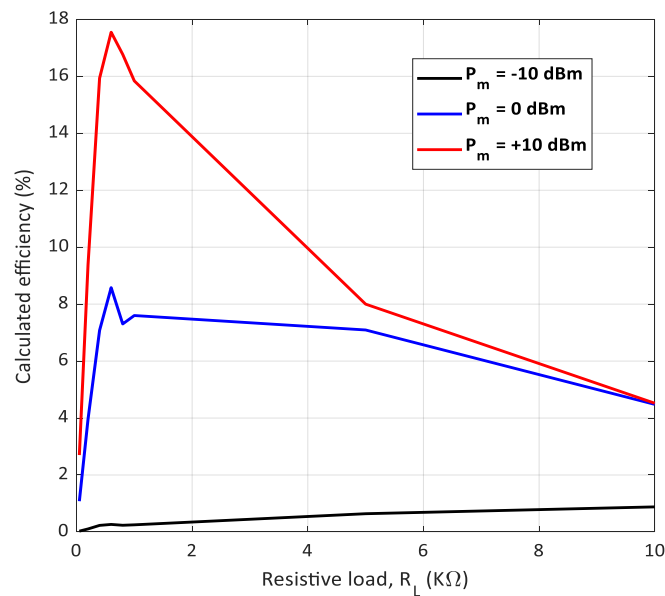
Figure 14. Efficiencies for different R_L and P_m for the rectifier circuit in Approach I.

3.1.3. The Stress Test

For the line-of-sight communication between the transmitter and the receiver, this test yielded an allowable limit of angular deviations from the line-of-sight orientation between the transmitter and the receiver for a successful event of WPT. During the stress test, the receiver (Rx) was moved from left to right in front of the transmitter (Tx) on a straight path, changing the distance from the center from -5 cm to 5 cm, with an interval of 1 cm. The test was performed for two cases, Case A and Case B, where the Tx power was 5 dBm and 15 dBm, respectively. The test setup is shown in Figure 15, where D_{Tx} is the distance of the transmitter from the center, and D_{Rx} is the distance from the receiver to the center position, along the orthogonal line. The received power for this stress test is shown in Figures 16 and 17, which gives us an idea of how much deviation could be allowed from the line-of-sight orientation during a WPT event.
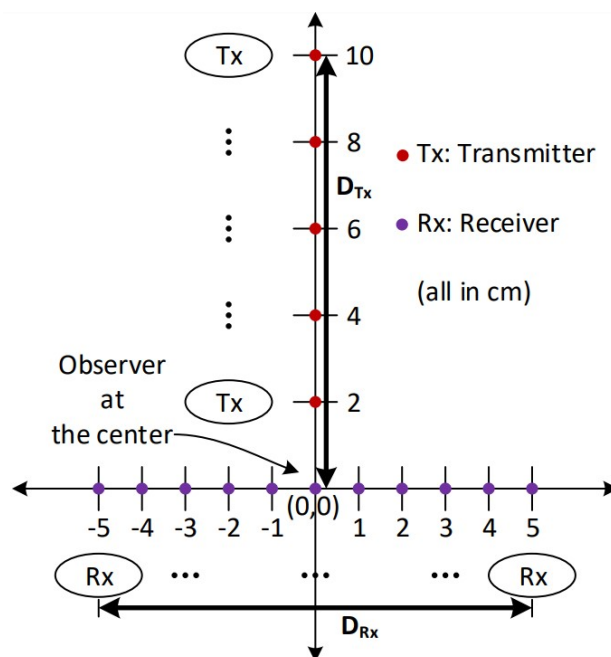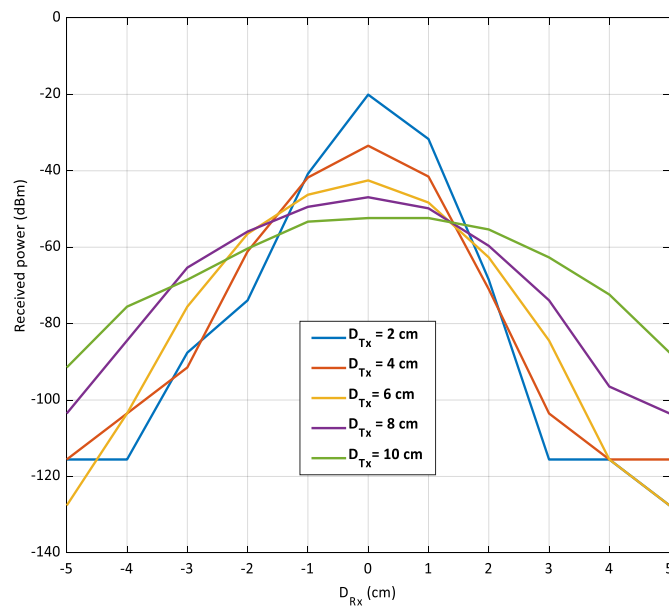

Figure 15. Setup to perform a stress test.

Figure 16. Stress test for Case A (P_{in} = 5 dBm, R_L = 0.6 kΩ).

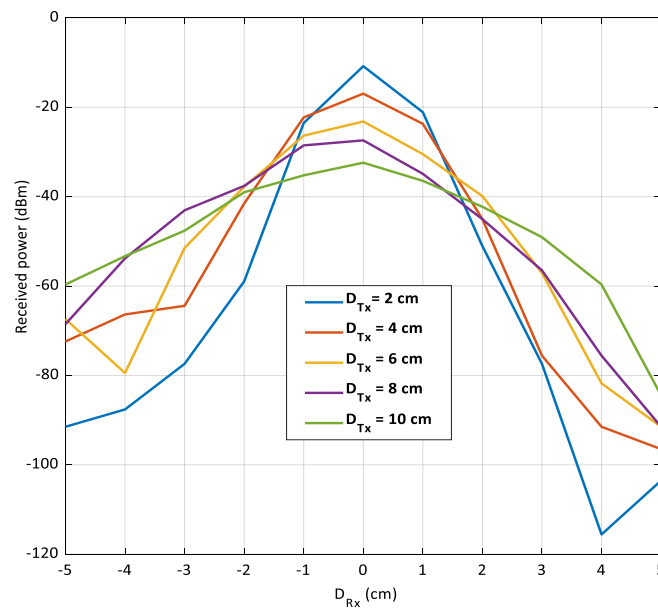**Figure 17.** Stress test for Case B (P_{in} = 15 dBm, R_L = 0.6 kΩ).

3.1.4. The System Test

The system test, as shown in Figure 18, was performed to measure the received power at a line-of-sight (0° angle) and at different transmitted powers. D is the distance between the Tx (MPAA) and the Rx (MPA). The measurements were performed at different D (1 cm to 20 cm) against a constant load of 0.6 kΩ at the ISM frequency band (2.4 GHz). Please note that all the losses, including approximately 3 dB loss of cable, are included in this measurement.

The measured DC voltages for two different input transmitted powers, P_{in} and various D, are presented in Figure 19. In addition, the measured power at the receiving end for different input powers is plotted in Figure 20. The target was to get at least 0.5 mW of power. Table 2 summarizes the received power levels over various distances. The highest received power, −2.97 dBm or 0.504 mW, was achieved, while the transmitted power P_{in} was 15 dBm over a distance of 1 cm.

Table 2. Summary of the Received Power of the Proposed WPT System.

Transmitted Power (dBm)	Highest Received Power (dBm)	D (cm)
5	−9.54	1
15	−2.97	1
	Lowest Received Power (dBm)	
5	−37.78	20
15	−29.38	20
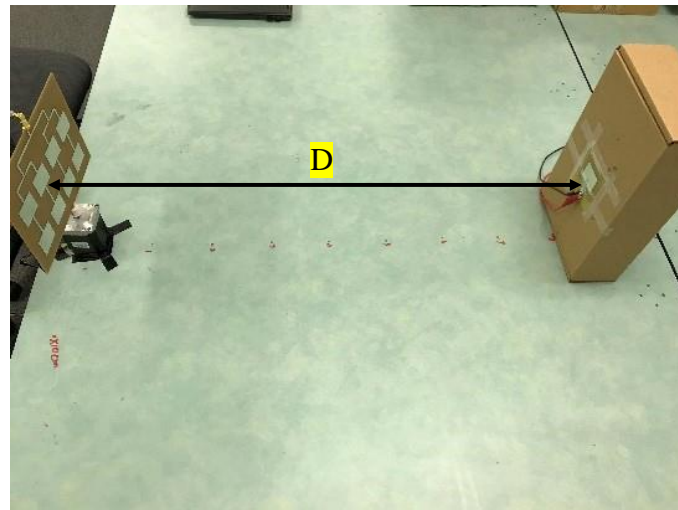
Figure 18. Measurement setup to perform system test, D is the distance between the Tx (MPAA) and the Rx (MPA).
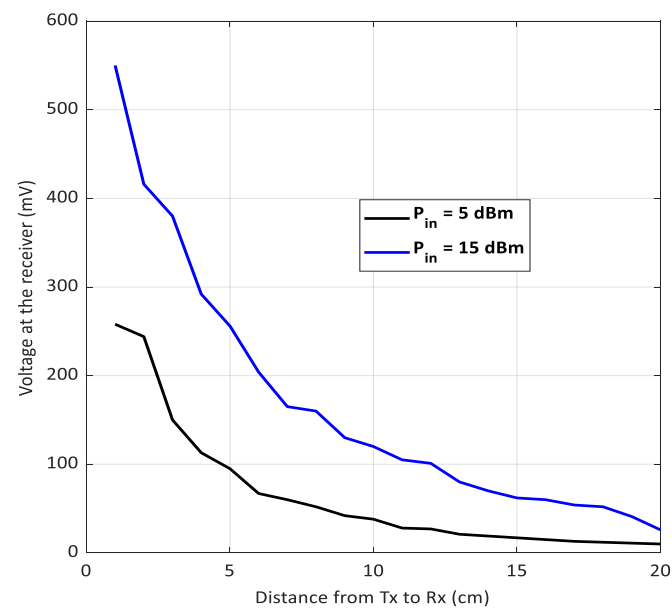
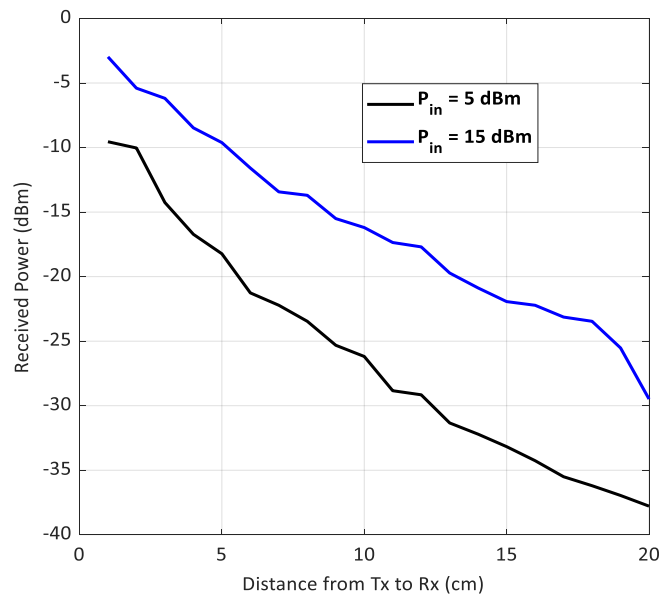**Figure 19.** Measured voltage at receiver end for the input transmitter power of 5 dBm and 15 dBm.

Figure 20. Received power for the input transmitter power of 5 dBm and 15 dBm.

3.2. Approach II

3.2.1. Antennas

The transmitter and receiver antennas in this approach are both BSPA, as was shown in Figure 5. The simulated and measured reflection coefficients are shown in Figure 21, and the simulated and measured radiation patterns are shown in Figure 22.

The transmitter antenna is fed through the Butler matrix, and depending on the input of the Butler matrix, four beams with around 22.5° angle differences can be created, as shown in Figure 23. As can be seen, the receiver antenna has a wide beam, and this allows for a small angular spread of the receivers, while the transmitter power is focused on one area at a time, reducing the waste of power in the angles that are not of interest.
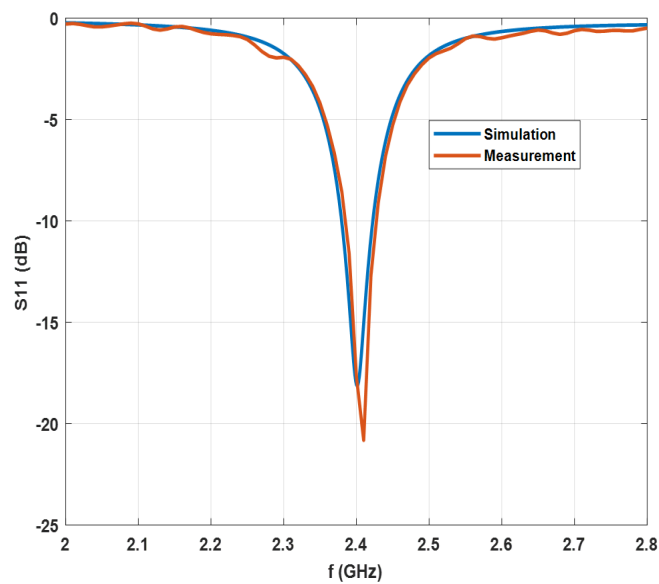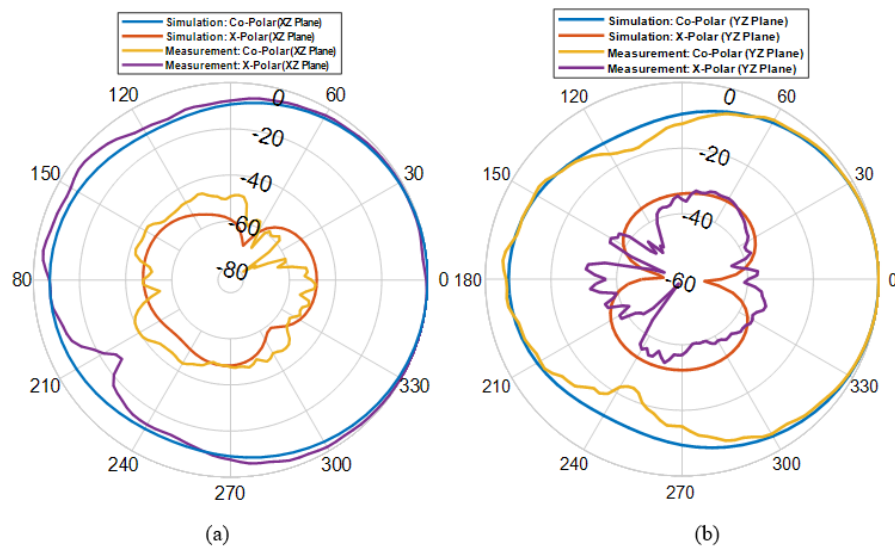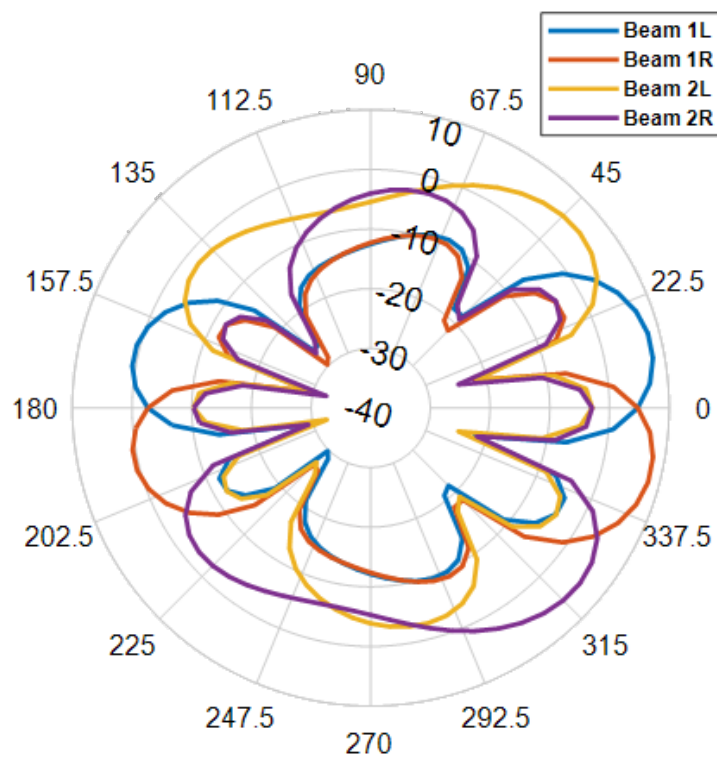

Figure 21. Simulated and measured reflection coefficient ($|S_{11}|$) of the BSPA.

Figure 22. Simulated and measured radiation patterns of the single antenna at 2.4 GHz, (**a**) $\phi = 0°$, (**b**) $\phi = 90°$.

Figure 23. Radiation pattern for each state of Butler matrix.

3.2.2. The Butler Matrix

As mentioned, the Butler matrix is used to rotate the beam to predefined angles. The Butler matrix was simulated, fabricated, and measured. Figure 24 shows S-plots of the implemented Butler matrix. As can be seen from the S_{11} and S_{22} plots, a good match has been achieved. In addition, S_{15} and S_{26} are about -6 dB, showing the power division to the four output ports.
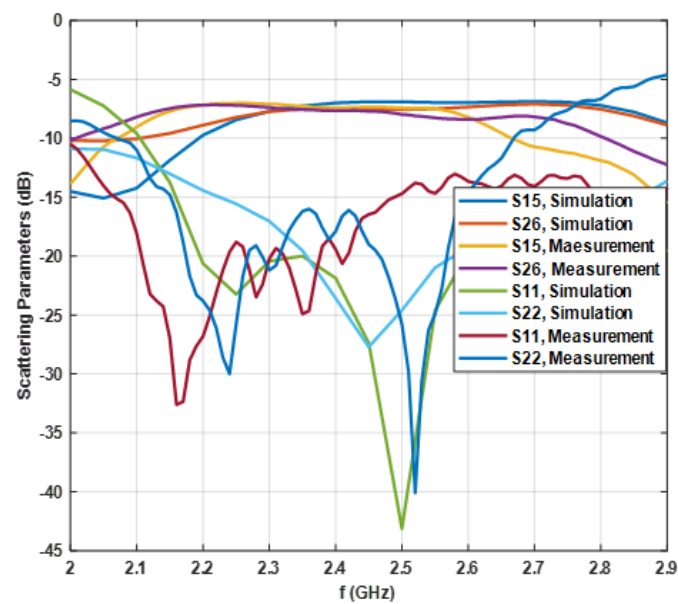
Figure 24. Scattering parameters for the proposed Butler matrix.

3.2.3. The Rectifier

Similar to the first approach for the rectifier, we used a Schottky Diode, Broadcom HSMS-2822, which is suitable for high-power design in a strong RF environment. A simple L-shaped lumped element matching is used for tuning the circuit after fabrication. We have used Cadence AWR software to simulate and design the rectifier circuit as well as the matching circuit.

3.2.4. The Mobile App

To design the mobile app, we used MIT APP Inventor. MIT App Inventor is an intuitive visual programming environment that allows everyone to build fully functional apps for android-based smartphones and tablets [21]. Figure 25 shows three main pages, a graph, and Help for the app. To use this app, first, the Bluetooth connection should be established, and then, the commands for turning on and off the system (RFin), and controlling switching times can be sent.
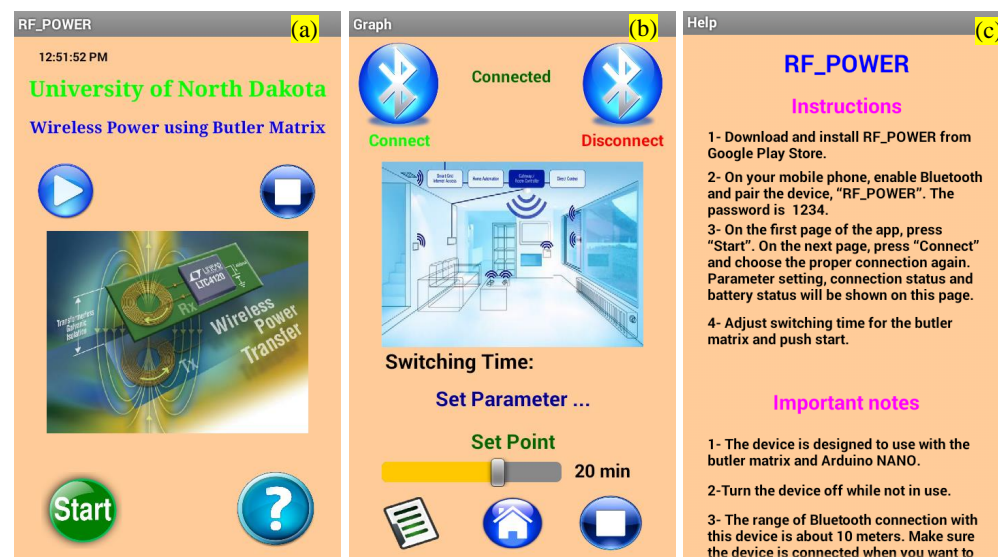

Figure 25. Mobile app for the RF power transfer system design. (**a**) Frontpage, (**b**) Timer set, and Bluetooth connection page, (**c**) Instruction page.

3.2.5. System Test

Figure 26 shows the output DC voltage versus the received input power (P_r) for various loads. Figure 27 shows the rectifier efficiency versus the received power (P_r) for various loads.

The overall system with the rectifier attached to the receiver antenna and the Butler matrix attached to the transmitter antenna was tested for a 62 kΩ load resistance. Figure 28 shows the measured output voltage for each beam. For Approach II, the measured output voltage for each beam is shown in Figure 28.
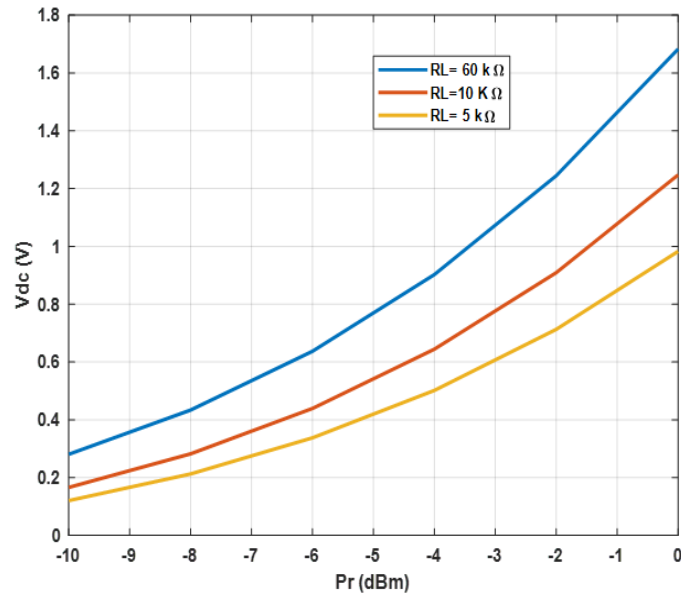

Figure 26. Output voltage at the load for different R_L and P_r, for the rectifier circuit in Approach II.
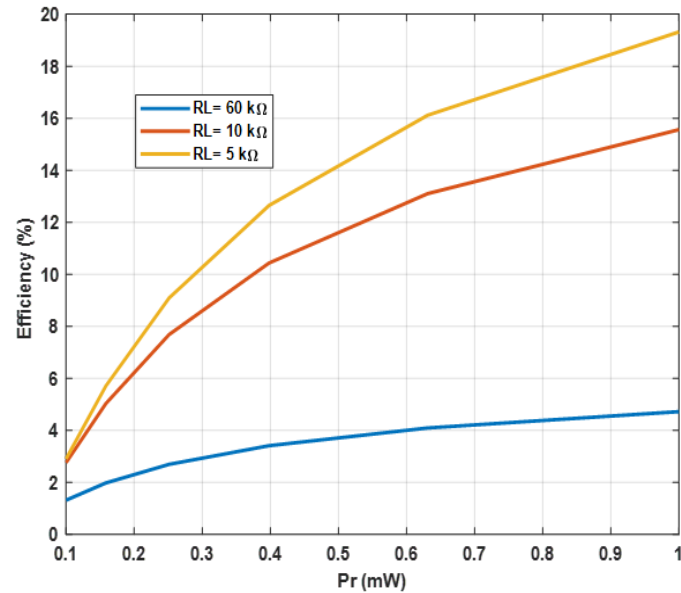

Figure 27. Efficiencies for different R_L and P_r for the rectifier circuit in Approach II.
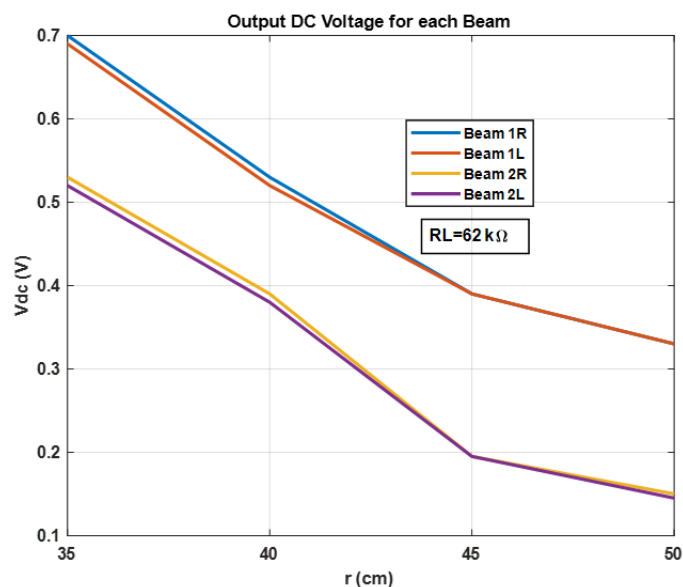
Figure 28. Measurement of maximum DC voltage for four output positions.

4. Conclusions

This paper proposes a radiative wireless power transfer using high-gain narrow beam antenna arrays. Two approaches are proposed. The performances of both approaches were studied. In the first approach, the microstrip patch array was mounted on a small stepper motor and controlled to rotate the array toward the desired angle. A microstrip patch antenna was integrated with a rectifier circuit to be used at the receiver. The rectifier circuit showed the best result of 17.03% efficiency for 0.6 kΩ, while the input power was 10 dBm. The system's efficiency was analyzed by changing the distance between the transmitter and receiver for different transmitted power levels at 2.4 GHz. A power of −2.97 dBm DC was received at a distance of 1 cm for a total input power of 15 dBm; this value includes all of the antenna and cable losses. The cable loss was estimated at about 3 dB. The WPT system's tolerance for variation was also determined by performing a stress test. The second approach used a Butler matrix to electronically control the beam and to rotate the main beam of a 1×4 Tx antenna. A butterfly-shaped patch antenna was designed and used for the receiver. This approach can provide four beams of power transfer at an angular difference of around 22.5°. A mobile app can control the direction of the beam and the time of switching the beam. A power transfer efficiency of 19% was achieved.

The two approaches that are proposed here provide simple methods of directing the beam toward the specified angles where the IoT devices are located. Using the first approach, a complete coverage of 360° is achievable. In the second approach, up to four simultaneous beams can be created and selected. The duration and the period of charging the IoT device can be controlled via a smartphone app.

Author Contributions: Conceptualization, S.N. and A.A.L.-N.; methodology, S.N. and A.A.L.-N.; software, A.A.L.-N.; validation, A.A.L.-N., S.R. and S.N.; formal analysis, T.N. and S.R.; investigation, T.N., S.R., A.A.L.-N. and S.N.; resources, S.N. and S.R.; data curation, T.N., A.A.L.-N., S.R. and S.N.; writing—original draft preparation, T.N. and A.A.L.-N.; writing—review and editing, S.N. and S.R.; visualization, T.N., A.A.L.-N. and S.N.; supervision, S.N. and S.R.; funding acquisition, S.N. All authors have read and agreed to the published version of the manuscript.

Data Availability Statement: Not applicable.

Conflicts of Interest: The authors declare no conflict of interest.

References

1. Ahlgren, B.; Hidell, M.; Ngai, E. Internet of Things for Smart Cities: Interoperability and Open Data. *IEEE Internet Comput.* **2016**, *20*, 52–56. [CrossRef]
2. Park, J.; Tran, N.; Hwang, S.; Kim, D.; Choi, K. Design and Implementation of 5.8 GHz RF Wireless Power Transfer System. *IEEE Access* **2021**, *9*, 168520–168534. [CrossRef]
3. Hui, S.; Zhong, W.; Lee, C. A Critical Review of Recent Progress in Mid-Range Wireless Power Transfer. *IEEE Trans. Power Electron.* **2014**, *29*, 4500–4511. [CrossRef]
4. Clerckx, B.; Zhang, R.; Schober, R.; Ng, D.; Kim, D.; Poor, H. Fundamentals of Wireless Information and Power Transfer: From RF Energy Harvester Models to Signal and System Designs. *IEEE J. Sel. Areas Commun.* **2019**, *37*, 4–33. [CrossRef]
5. Liu, C.; Guo, Y.; Sun, H.; Xiao, S. Design and Safety Considerations of an Implantable Rectenna for Far-field Wireless Power Transfer. *IEEE Trans. Antennas Propag.* **2014**, *62*, 5798–5806. [CrossRef]
6. Tesla, N. Apparatus for Transmitting Electrical Energy. US Patent 1,119,732, 1 December 1914.
7. Brown, W.C. *Experimental Airborne Microwave Supported Platform*; Technical Report; Raytheon Co.: Burlington, MA, USA; Spencer Lab: Newark, DE, USA, 1965.
8. Khoury, P. A Power-efficient Radio Frequency Energy-harvesting Circuit. Master's Thesis, University of Ottawa, Ottawa, ON, Canada, 2013.
9. Ettorre, M.; Alomar, W.; Grbic, A. 2-D Van Atta Array of Wideband, Wide-angle Slots for Radiative Wireless Power Transfer Systems. *IEEE Trans. Antennas Propag.* **2018**, *66*, 4577–4585. [CrossRef]
10. Poveda-García, M.; Oliva-Sánchez, J.; Sanchez-Iborra, R.; Cañete-Rebenaque, D.; Gomez-Tornero, J. Dynamic Wireless Power Transfer for Cost-Effective Wireless Sensor Networks Using Frequency-Scanned Beaming. *IEEE Access* **2019**, *7*, 8081–8094. [CrossRef]
11. Hong, H.; Soo Park, H.; Hong, S. Design of Rotman Lens for Far-field Wireless Power Transfer at Ka-band. In Proceedings of the 2020 IEEE Wireless Power Transfer Conference (WPTC), Seoul, Korea, 15–19 November 2020.
12. Pabbisetty, G.; Murata, K.; Taniguchi, K.; Mitomo, T.; Mori, H. Evaluation of Space-time Beamforming Algorithm to Realize Maintenance-free IoT Sensors with Wireless Power Transfer System in the 5.7-GHz Band. *IEEE Trans. Microw. Theory Tech.* **2019**, *67*, 5228–5234. [CrossRef]
13. An, C.; Kwon, H.; Ryu, H. Beamforming Design of the Wireless Power Transfer System into Multiple IoT Sensors. In Proceedings of the 2022 24th International Conference On Advanced Communication Technology (ICACT), Phoenix Pyeongchang, Republic of Korea, 13–16 February 2022.
14. Bae, J.; Yi, S.; Koo, H.; Oh, S.; Oh, H.; Choi, W.; Shin, J.; Song, C.; Hwang, K.; Lee, K.; et al. LUT-Based Focal Beamforming System Using 2-D Adaptive Sequential Searching Algorithm for Microwave Power Transfer. *IEEE Access* **2020**, *8*, 196024–196033. [CrossRef]
15. Mansour, A.; Shehata, N.; Hamza, B.; Rizk, M. Efficient Design of Flexible and Low-cost Paper-based Inkjet-printed Antenna. *Hindawi Int. J. Antennas Propag.* **2015**, *2015*, 845042. [CrossRef]
16. Din, N.; Chakrabarty, C.; Ismail, A.; Devi, K.; Chen, W. Design of RF Energy Harvesting System for Energizing Low-power Devices. *Prog. Electromagn. Res.* **2012**, *132*, 49–69. [CrossRef]
17. Balanis, C. *Antenna Theory: Analysis and Design*, 4th ed.; Wiley-Interscience: Hoboken, NJ, USA, 2016; ISBN 978-1-118-64206-1.
18. Butler, J. Beam-forming Matrix Simplifies the Design of Electronically Scanned Antennas. *Electron. Des.* **1961**, *9*, 170–173.
19. Prakash, V.; Dahiya, S.; Kumawat, S.; Singh, P. Design of 4X4 Butler Matrix and Its Process Modeling using Petri-nets for Phase Array Systems. *Prog. Electromagn. Res. C* **2020**, *103*, 137–153. [CrossRef]
20. Sfar, I.; Osman, L.; Gharsallah, A. Design of a 4X4 Butler Matrix for Beamforming Antenna Applications. In Proceedings of the 2014 Mediterranean Microwave Symposium (MMS2014), Marrakech, Morocco, 12–14 December 2014.
21. Tutorials for MIT App Inventor. Available online: http://appinventor.mit.edu/explore/ai2/tutorials.html (accessed on 26 November 2022).